

MiniBooNE and Sterile Neutrinos

M. H. Shaevitz^{a*} for the BooNE Collaboration[1][†]

^aColumbia University, Department of Physics, New York, NY 10027

Sterile neutrinos may be an important extension to the standard model, and could both hold the key to understanding neutrino mass and mixing as well as play an important role in leptogenesis. In many models, the sterile neutrinos could be light and accessible to current and near term experiments. The MiniBooNE experiment is set up to explore these possibilities in the Δm^2 region from 0.3 to a few eV^2 where the LSND experiment has reported a $\bar{\nu}_e$ appearance signal. This report will outline some of these extensions, give the status and prospects for the MiniBooNE experiment, and explore future investigations if MiniBooNE sees an oscillation signal.

1. Extensions to the Neutrino Standard Model

The standard model has three flavors of massless Dirac neutrinos ν_e, ν_μ, ν_τ . The results of neutrino oscillation measurements over the last decade have required that this simple picture be modified to allow mixing between the flavors and to add mass for the neutrinos. These modifications have opened up many questions that are currently being pursued experimentally. The questions include: What are the number of neutrinos? Are the masses Majorana or Dirac? Does the neutrino mass hierarchy follow that of the charged leptons? Why are the mixings so different from the quark sector?

1.1. Extensions with Sterile Neutrinos

The current experimental measurements in the solar ($\Delta m_{Solar}^2 \approx 7 \times 10^{-5} \text{ eV}^2$) and atmospheric ($\Delta m_{Atmosph.}^2 \approx 2.5 \times 10^{-3} \text{ eV}^2$) regions combined with the LSND result ($\Delta m_{LSND}^2 = 0.3 - 3 \text{ eV}^2$) give three disparate mass squared differences. The three Δm^2 cannot be explained with only three types of neutrinos since

$$\Delta m_{LSND}^2 \neq \Delta m_{Solar}^2 + \Delta m_{Atmosph.}^2.$$

Only-three models, where the atmospheric oscillations correspond to a mixture of oscillations at the Δm_{Solar}^2 and Δm_{LSND}^2 scales, are strongly disfavored by the current data since these models

would demand a strong ν_e appearance signal that is not seen in the Super-K atmospheric data.

The solution to this inconsistency opens many possibilities. First, one of the experimental measurements could be wrong. The recent results from the SNO and Kamland experiments have substantiated the oscillation interpretation of the solar neutrino deficit, and the K2K experiment, although with large uncertainties, has seen a disappearance signal in the Super-K atmospheric region. MiniBooNE is in the process of exploring oscillations in the LSND region and will make a definitive check of the LSND anomaly.

Another possibility is that one of the experiments is not seeing neutrino oscillations but the results of another type of process such as neutrino decay; or, for example, for LSND, neutrino production from a lepton flavor violating decay. It also may be possible that this inconsistency has its origin in CPT violation which could imply that oscillations may be different for neutrinos and antineutrinos. The recent confirmation by Kamland of oscillations in the solar region using reactor antineutrinos limits any CPT interpretation for the solar region. In the future, the MINOS experiment will be able to check CPT invariance for the oscillations in the atmospheric region by performing separate measurements with neutrinos and antineutrinos.

An elegant solution that could explain the three distinct mass differences is the addition of one or more sterile neutrinos. Sterile neutrinos are natural extensions to the standard model, and are

*shaevitz@nevis.columbia.edu

[†]This work supported by the NSF and DOE.

demanded in many grand-unified theories, extra-dimension theories, and various types of lepton symmetry models. A confirmation that sterile neutrinos exist would have a major impact on our understanding of the neutrino sector and have far reaching effects on building models from unification to cosmology. Also, additional sterile neutrinos could be a significant source of measurable CP violating effects and will make the neutrino oscillation phenomenology much more diverse.

The phenomenology for adding extra sterile neutrinos involves broadening the mixing matrix and adding new extra mass values. The sterile neutrinos are weak isospin singlets and thus do not couple to either the standard W or Z bosons. Sterile neutrinos would therefore evade the LEP bound on the number of light active neutrinos, and the detection of sterile neutrino effects could only take place through mixing with the standard active neutrinos. In the 3+1 and 3+2 schemes, additional sterile states are added with masses corresponding to the Δm_{LSND}^2 region. The high mass states are mainly composed of sterile components but can have small admixtures of active states as shown in Figure 1. The extended neutrino mixing matrix is shown in Figure 2, where the upper left 3×3 components correspond to the usual active neutrino mixing matrix and the $U_{e4(5)}$ and $U_{\mu4(5)}$ components would contribute to an LSND ν_e appearance signal through oscillation through the sterile neutrinos.

A sterile neutrino has also been proposed to explain some small solar neutrino discrepancies such as the argon neutrino rate being two sigma smaller than expected and the lack of an upturn in the Be neutrino rate at low energies[2]. Sterile neutrinos may also be important in contributing to the rapid-neutron-capture process (r-process) in heavy element production by supernovae[3]. The observed abundance of heavy elements is much larger than standard model predictions where the heavy element production is limited by the small size of the the neutron density. The neutron density can be increased in a model where matter effects cause more ν_e 's to oscillate to sterile neutrinos than $\bar{\nu}_e$'s. The excess of the $\bar{\nu}_e$'s then produces a substantial neutron excess through the inverse beta decay process.

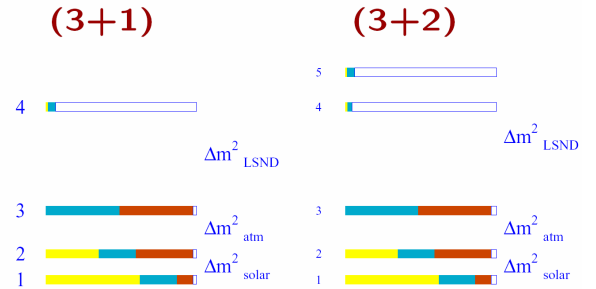


Figure 1. Example flavor compositions of the neutrino mass eigenstates for a 3+1 and 3+2 model with extra sterile neutrinos. The composition of each mass state is given by the colored bars with electron-type (yellow), muon-type (blue), tau-type (red), and sterile-type (white).

$$\begin{pmatrix} \nu_e \\ \nu_\mu \\ \nu_\tau \\ \nu_s \\ \nu_{s'} \\ \vdots \end{pmatrix} = \begin{pmatrix} U_{e1} & U_{e2} & U_{e3} & U_{e4} & U_{e5} & \dots \\ U_{\mu1} & U_{\mu2} & U_{\mu3} & U_{\mu4} & U_{\mu5} & \dots \\ U_{\tau1} & U_{\tau2} & U_{\tau3} & U_{\tau4} & U_{\tau5} & \dots \\ U_{s1} & U_{s2} & U_{s3} & U_{s4} & U_{s5} & \dots \\ U_{s'1} & U_{s'2} & U_{s'3} & U_{s'4} & U_{s'5} & \dots \\ \dots & \dots & \dots & \dots & \dots & \dots \end{pmatrix} \begin{pmatrix} \nu_1 \\ \nu_2 \\ \nu_3 \\ \nu_4 \\ \nu_5 \\ \vdots \end{pmatrix}$$

Figure 2. The neutrino mixing matrix for a 3+n model with extra sterile neutrinos, ν_s and $\nu_{s'}$.

Big-bang nucleosynthesis and the anisotropy measurements of the cosmic microwave background give constraints on the number of neutrinos including sterile neutrinos. Standard cosmological models using current measurements constrain the total number of neutrinos to be 2.6 ± 0.4 which can be somewhat relaxed to 4.0 ± 2.5 if the systematic uncertainty on the ${}^4\text{He}$ abundance is larger. These cosmological constraints can be evaded if the neutrinos have a lepton asymmetry or if equilibrium assumptions are not valid[4]. In fact, Hannestad has claimed that “the LSND result is not yet ruled out by cosmological observations” and has shown how the cosmological mass bounds would be increased from $\Sigma m_{\nu_i} = 1.0$ to 1.4 (2.5) eV if there are four (five) neutrinos instead of the usually assumed three[5].

1.2. 3+1 and 3+2 Global Fits to Neutrino Oscillation Results

There have been many searches for neutrino oscillations in the high mass Δm^2 region associated with the LSND result including the KARMEN, NOMAD, Bugey, CHOOZ, CCFR84, and CDHS experiments. These experiments have set both appearance and disappearance limits on oscillations at various levels. Global fits[6] to these null short-baseline (NSBL) experiments plus the LSND signal have been performed to determine the allowed regions in oscillation parameter space and answer the question if there are regions of compatibility. In these fits, LSND is the only positive signal (at the 3.8σ level), but the CDHS experiment also shows a two sigma deficit in the near detector.

From fits to 3+1 models, a compatibility (calculated from $1 - \delta_{\text{NSBL}}(\delta_{\text{LSND}} + (1 - \delta_{\text{LSND}})/2)$) of 3.6% between LSND and the NSBL experiments is obtained with the overlap regions shown in Figure 3. (δ_{NSBL} and δ_{LSND} are the confidence levels of the fit for the NSBL and LSND data respectively.) This value of compatibility does not support any conclusive statement, although it represents poor agreement between the LSND and NSBL data sets. Assuming compatibility, the allowed regions in parameter space are shown in Figure 4 with best fit values for the parameters of $\Delta m_{41}^2 = 0.92$ eV² with $U_{e4} = 0.136$ and $U_{\mu 4} = 0.205$. The

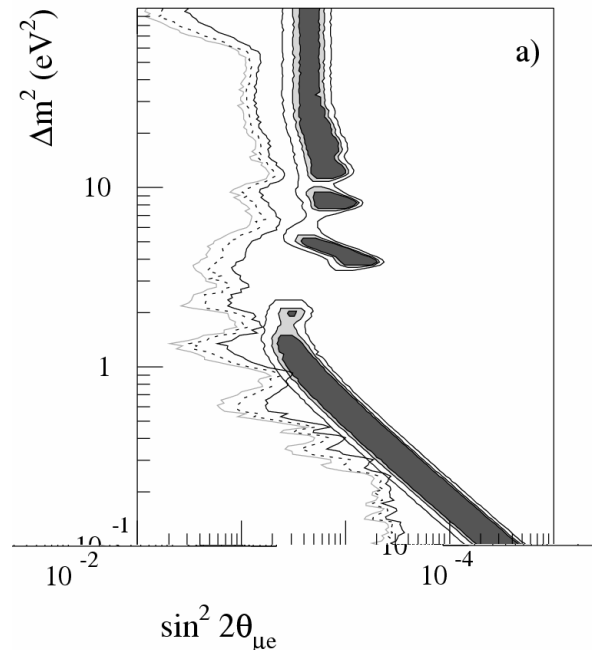


Figure 3. Compatibility between NSBL and LSND datasets in (3+1) models. The figure shows the 90% (grey solid line), 95% (black dotted line), and 99% (black solid line) CL exclusion curves ($\sin^2 2\theta_{\mu e}, \Delta m^2$) space for (3+1) models, considering the NSBL experiments. Also shown are the 90%, 95%, and 99% CL allowed regions for the LSND data.

global χ^2 minimum is $\chi_{\text{SBL}}^2 = 144.9$ (148 d.o.f.) with the individual NSBL and LSND contributions being $\chi_{\text{SBL}}^2 = 137.3$ and $\chi_{\text{LSND}}^2 = 7.6$, respectively.

The (3+2) model fits give much better compatibility than the (3+1) fit, beyond what would be the statistical expectation for adding an additional three parameters associated with the second sterile neutrino, Δm_{51}^2 , U_{e5} and $U_{\mu 5}$. Since two parameter representations in terms of $\sin^2 2\theta_{\mu e}$ and Δm^2 are not possible in a (3+2) model, the results of the 3+2 fits are displayed in terms of the parameter, p_{LSND} , the probability

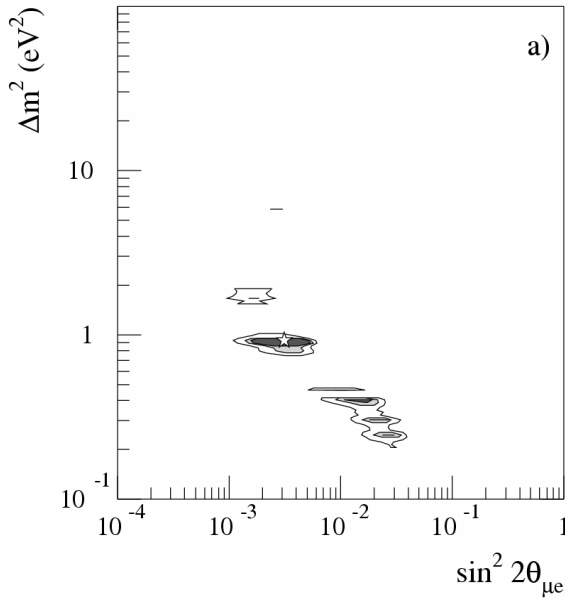


Figure 4. Allowed regions in parameter space from a combined analysis of NSBL and LSND data, in (3+1) models, assuming statistical compatibility of the NSBL and LSND datasets. The figure shows the 90%, 95%, and 99% CL allowed regions in $(\sin^2 2\theta_{\mu e}, \Delta m^2)$ space, together with the best-fit point, indicated by the star.

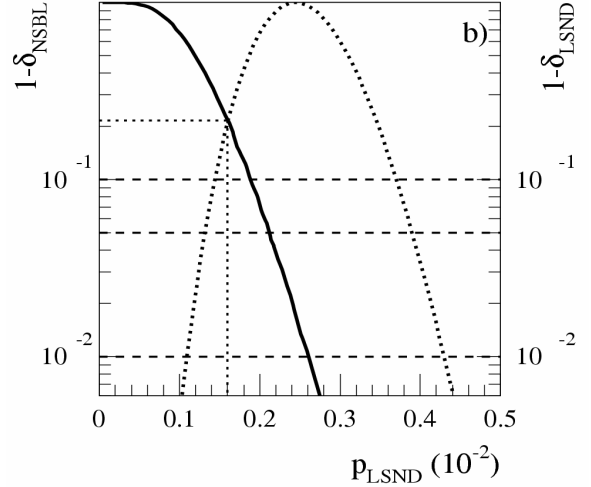


Figure 5. Individual confidence levels δ_{NSBL} and δ_{LSND} , as a function of the LSND oscillation probability p_{LSND} , for the NSBL and LSND datasets. The curves are for (3+2) models with the neutrino mass splittings, Δm_{41}^2 and Δm_{51}^2 , fixed to the best-fit values $\Delta m_{41}^2 = 0.92 \text{ eV}^2$, $\Delta m_{51}^2 = 22 \text{ eV}^2$ from the combined NSBL+LSND analysis, and variable mixing matrix elements U_{e4} , $U_{\mu 4}$, U_{e5} , $U_{\mu 5}$. The left curve refers to the NSBL dataset, the right one to the LSND dataset.

of giving $\nu_{\mu} \rightarrow \nu_e$ transitions for the LSND L/E distribution. From Figure 5 which shows a maximum compatibility at $\delta_{\text{NSBL}} = \delta_{\text{LSND}} = 0.785$, one obtains a compatibility value of 30% as compared to the 3.6% for the (3+1) models.

Fig. 6 shows the 90% and 99% CL allowed regions in $(\Delta m_{41}^2, \Delta m_{51}^2)$ space obtained in the combined (3+2) analysis. In light of the (3+1) analysis, the result is not surprising, pointing to favored masses in the range $\Delta m_{41}^2 \simeq 0.9 \text{ eV}^2$, $\Delta m_{51}^2 \simeq 10 - 40 \text{ eV}^2$, at 90% CL. At 99% CL, the allowed region extends considerably, and many other $(\Delta m_{41}^2, \Delta m_{51}^2)$ combinations appear. The best-fit model ($\chi_{\text{SBL}}^2 = 135.9$, 145 d.o.f.) is described by the following set of parameters: $\Delta m_{41}^2 = 0.92 \text{ eV}^2$, $U_{e4} = 0.121$, $U_{\mu 4} = 0.204$,

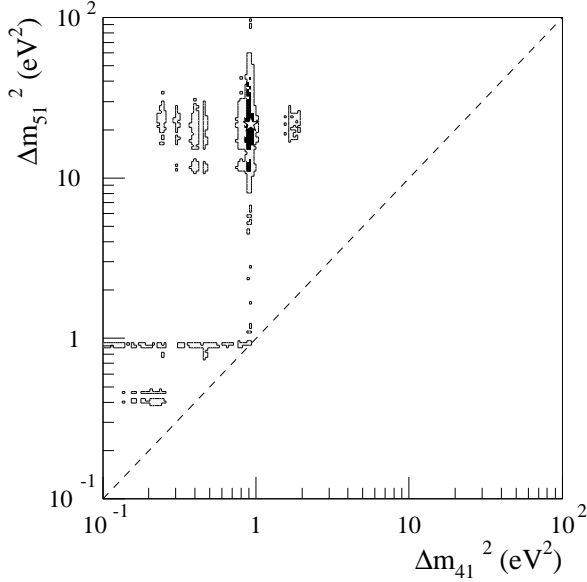


Figure 6. Allowed ranges in $(\Delta m_{41}^2, \Delta m_{51}^2)$ space for (3+2) models, for the combined NSBL+LSND analysis, assuming statistical compatibility between the NSBL and LSND datasets. The star indicates the best-fit point, the dark and light grey-shaded regions indicate the 90 and 99% CL allowed regions, respectively.

$\Delta m_{51}^2 = 22 \text{ eV}^2$, $U_{e5} = 0.036$, and $U_{\mu 5} = 0.224$. Solution with sub-eV neutrino masses are also possible and the best fit value for these is given by: $\Delta m_{41}^2 = 0.46 \text{ eV}^2$, $U_{e4} = 0.090$, $U_{\mu 4} = 0.226$, $\Delta m_{51}^2 = 0.89 \text{ eV}^2$, $U_{e5} = 0.125$, $U_{\mu 4} = 0.160$, corresponding to $\chi_{\text{SBL}}^2 = 141.5$ (145 d.o.f.).

2. MiniBooNE and Sterile Neutrinos

MiniBooNE will be one of the first experiments to check such sterile neutrino models. The experiment will make a definitive investigation of the LSND anomaly to determine if it is from neutrino oscillations and, if so, measure the oscillation parameters. In addition, MiniBooNE will look for sterile neutrinos through searches for a ν_{μ} disappearance signal.

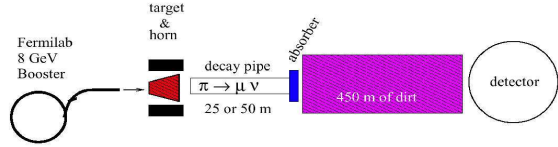


Figure 7. Schematic diagram of the MiniBooNE beamline. Protons from the Fermilab 8 GeV Booster are focused onto a 1.7 interaction length beryllium target. A magnetic horn then focuses positive (or negative) pions into a 50 m long decay pipe. Following a steel dump at the end of the decay pipe is 490 m of dirt shield before the MiniBooNE detector.

2.1. The MiniBooNE Experiment

In order to test the LSND result, MiniBooNE is designed to sample an L/E region similar to the LSND value of $1\text{m}/\text{MeV}$ while substantially changing the sources and size of systematic errors. In addition, MiniBooNE will have superior statistics allowing the experiment to make a definitive statement as to whether oscillations exist in this region. To accomplish these goals, the 450-ton MiniBooNE detector is located at $L = 541 \text{ m}$ from the production target, and the neutrino flux is produced from 8 GeV Fermilab Booster protons impinging on a beryllium target giving neutrinos with a mean energy around 800 MeV. Compared to LSND, MiniBooNE neutrinos are produced from energetic (not stopping) pions and the signature and backgrounds for $(\bar{\nu}_e)$ appearance are much different. As shown in Figure 7, the neutrino beam is produced by pion and kaon decays in a 50 m decay region downstream of single, magnetic-horn focusing system. The proton beam arrives at the production target within the horn during $1.6 \mu\text{s}$ beam spills that happens at about 5 Hz.

The MiniBooNE detector shown in Figure 8 consists of a 12.2 m diameter tank filled with pure mineral oil with the outer surface lined with 1280 photomultiplier tubes (PMTs). The fiducial vol-

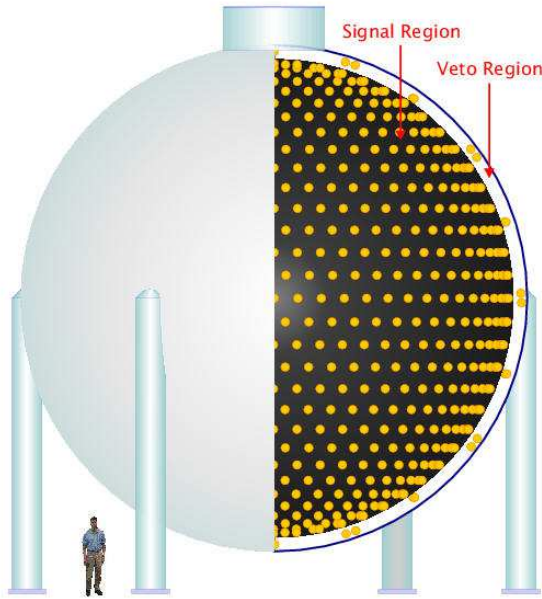


Figure 8. A schematic diagram of the MiniBooNE detector showing the signal and veto regions. Each filled circle corresponds to a photomultiplier tube. The veto region is isolated from the signal region by an optical barrier.

ume corresponds to 450 tons of oil and is defined by a veto region instrumented with 240 PMTs at the outer radii. Neutrinos are identified and measured using the Cerenkov and the small amount of scintillation light produced by outgoing charged tracks. The interaction point, time of an event, and the directions of relativistic tracks are reconstructed from the time and charge recorded in the PMTs.

Particle identification is accomplished with a neural net that uses the difference in characteristics of the Cerenkov rings and scintillation light associated with electrons, muons, protons, or π^0 's. Most muon neutrino events can be easily identified by their penetration into the veto region or by their stopping and producing a Michel electron after a few microseconds. An important

background to the ν_e appearance search is ν_μ neutral current production of π^0 's, most of which are identified by the production of two Cerenkov rings from the two decay gamma-rays.

Simple cuts requiring that a candidate neutrino event have a time within the $1.6\mu\text{s}$ beam spill, fewer than 6 veto hits, and more than 200 signal region hits reduces cosmic ray background to 1 in 1000 with respect to beam events. The beam that arrives at the detector is almost all ν_μ 's with a small 0.6% contamination of ν_e 's that mainly come from muon and kaon decay in the decay pipe. Even though the kaon contribution is smaller than the muon, the uncertainty in kaon production is a dominant systematic uncertainty in the ν_e appearance oscillation measurement.

Several methods are used to calibrate the detector over the full energy range from 50 to 1000 MeV. The spectrum of observed Michel electrons from stopped muon decay yields a calibration point at the 53 MeV Michel endpoint. Figure 9 shows good agreement between the data and expectation with an energy resolution of 15% at 53 MeV. Cosmic ray muons also provide an energy calibration when their path length can be identified. To accomplish this, a multi-plane, scintillator hodoscope on the top of the detector is combined with scintillating cubes placed at various locations in the tank. Using this combination, a series of muon ranges corresponding to energies of 100 to 1000 MeV can be isolated and used for calibration.

Reconstructed π^0 events provide yet another calibration source. Figure 10 shows a preliminary invariant mass distribution for events with two Cerenkov rings above 40 MeV. The photons that are included in the pion mass distribution span a considerable range from 40 to over 1000 MeV. The agreement of the mass peak at 136.3 ± 0.8 MeV with the 135.0 MeV expectation then gives a check on the energy scale over this range of photon energies.

2.2. Oscillation Analysis: Status and Plans

The MiniBooNE collaboration is committed to performing a “closed box” analysis for the ν_e appearance search. For this procedure, the data events that could contain electron neutrinos in

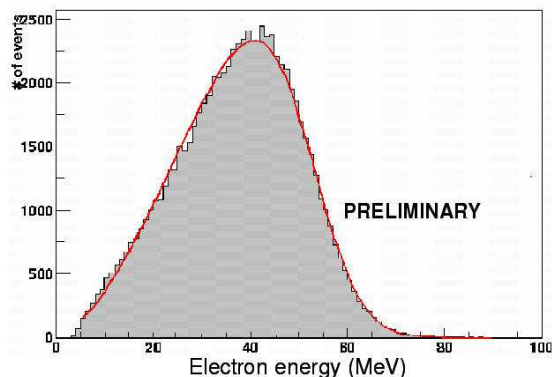


Figure 9. The Michel electron energy spectrum. The solid line is the expected spectrum convolved with a Gaussian resolution factor. The distribution at the endpoint indicates a 14.8% energy resolution.

the oscillation signal region are separated off and not available for full detailed analysis. In this way, inadvertent biases that might be introduced during the reconstruction development, tuning, and calibration can be avoided. Data events in other categories such as muon and NC π^0 events are available for study. The plan is to complete the full development, calibration, and verification of the event reconstruction with Monte Carlo and the “open data” before considering the “closed box” events.

The open data samples are already yielding interesting physics studies as well as serving as a cross check of the data reconstruction. These studies include a ν_μ disappearance oscillation search, measurements of cross sections for low-energy processes, studies of ν_μ NC π^0 production, and studies of ν_μ NC elastic scattering.

A more detailed report on the status and plans for the MiniBooNE physics analyses can be found in the “MiniBooNE Run Plan”[7] that was submitted to Fermilab in November 2003.

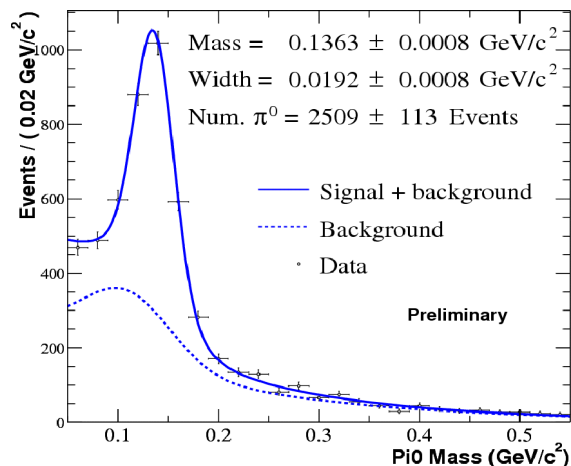


Figure 10. Reconstructed invariant mass for beam triggers satisfying “good event” selection cuts plus a > 40 MeV cut for each of the two assumed Cerenkov rings. The data are shown by the points and the Monte Carlo prediction for neutral current π^0 production and other backgrounds by the solid and dashed curves, respectively.

2.2.1. ν_μ Disappearance Search

The ν_μ disappearance search mainly uses quasi-elastic, charged-current (CC) events, $\nu_\mu + n \rightarrow \mu^- + p$. These events are isolated by identifying a single ring topology and PMT hit timing cuts. For quasi-elastic events, the incoming neutrino energy can be simply estimated from the energy and angle of the outgoing muon (or electron) using the formula:

$$E_\nu^{QE} = \frac{1}{2} \frac{2ME_\mu - m_\mu^2}{M - E_\mu + p_\mu \cos \theta_\mu}$$

From Monte Carlo studies, this procedure yields an energy resolution of about 10% at 800 MeV. With only a single detector, the oscillation search is performed by comparing the shape of the energy distribution to the Monte Carlo expectation. The Monte Carlo expectation has inputs from measured pion production experiments for energies around 8 GeV and from quasi-elastic cross section measurements. With an early data sample of 30,000 ν_μ CC quasi-elastic events, Figure 11 shows a comparison of the measured quasi-elastic energy, E_ν^{QE} , distribution in the data to Monte Carlo (each normalized to unit area). The error bars on the Monte Carlo include the current assessment of the major sources of systematic uncertainties. In particular, the errors include uncertainties associated with the ν_μ flux, ν_μ CC quasi-elastic cross section, and the properties of light production and transmission in the MiniBooNE detector. Substantial reductions of these uncertainties are expected as the analysis progresses. With the full data sample of several hundred thousand ν_μ CC quasi-elastic events, the estimated sensitivity to a disappearance signal is shown in Figure 12 along with the allowed regions from the previously described (3+1) sterile neutrino model fits. As that figure shows, the MiniBooNE measurement will address important regions for the (3+1) and therefore also the (3+2) models.

2.2.2. The $\nu_\mu \rightarrow \nu_e$ Appearance Search

A prime goal of MiniBooNE is to make a definitive search for neutrino oscillations in the LSND parameter region by looking for an anomalous signal of ν_e appearance over background. The

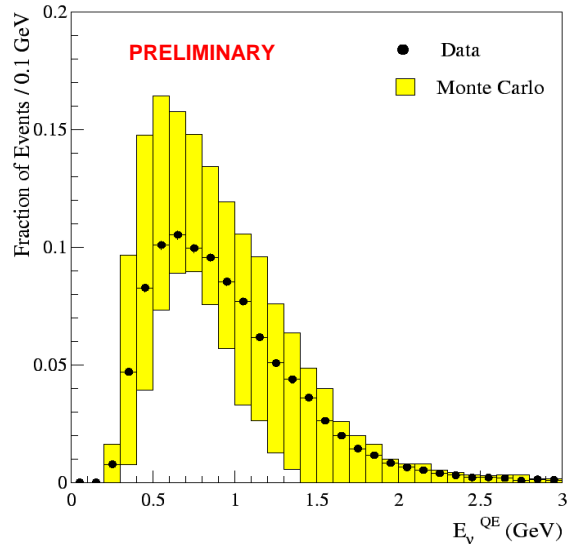


Figure 11. Reconstructed energy distribution for ν_μ charged-current, quasi-elastic events, data (black dots) and an example of the Monte Carlo prediction with optical model variations. (boxes). The distributions are normalized to unit area and, thus, only display shape information.

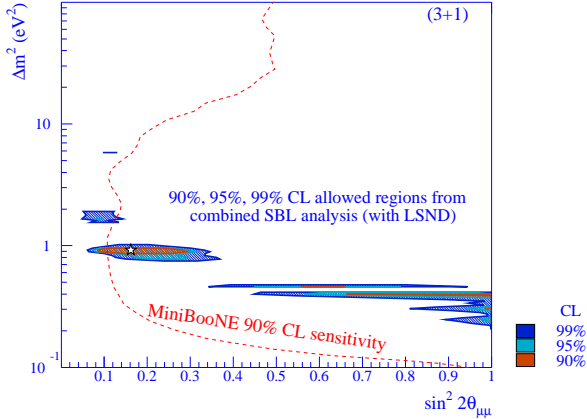


Figure 12. 90% CL sensitivity for a MiniBooNE ν_μ disappearance search with 1×10^{21} protons on target. Also shown are the 90%, 95%, and 99% CL regions from the (3+1) global fits to the NSBL and LSND data.

beam and detector have been designed to cover this region with good ν_e efficiency while minimizing backgrounds. An important feature of the MiniBooNE design is to constrain all backgrounds through either internal or external data measurements as outlined below. For 1×10^{21} protons on target, the expected number of oscillation and background events is given in Figure 13.

One of the major sources of background events is the intrinsic electron neutrinos in the beam. This background ν_e flux comes from muon and kaon decay and is at the 6×10^{-3} level with respect to the ν_μ event rate. For the ν_e 's from μ -decay, the flux is directly tied to the observed ν_μ flux, since the MiniBooNE detector only subtends neutrinos from very forward pion decays. The pion energy distribution can then be determined from the observed ν_μ events and used to predict the ν_e 's from μ -decay. The other major source of ν_e 's is from K_{e3} decay. This source will be determined using data from two low energy production experiments that have recently taken data, the HARP experiment at CERN[8]

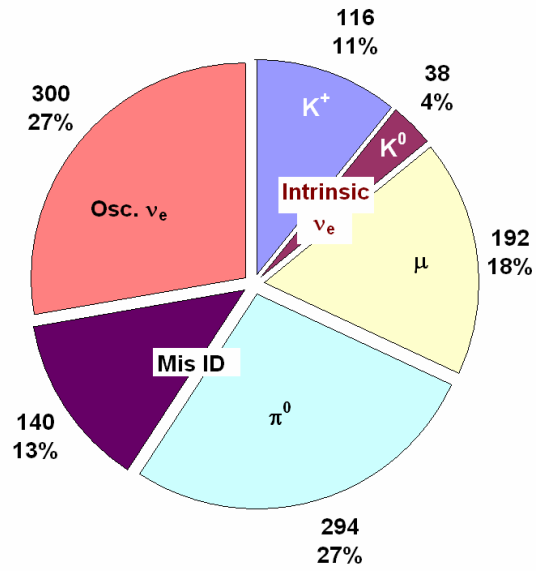


Figure 13. Statistics for various signal and background event categories. The numbers are for 1×10^{21} protons on target and are based on the observed neutrino flux. The number of oscillation events as shown is for the mid-range of the LSND allowed region and may vary by about 20% with the specific Δm^2 value.

and the E910 experiment at BNL[9]. With these production data, it is estimated that the ν_e flux from kaon decay can be determined with about a 5% uncertainty. An additional check will also be available from a special system, the Little Muon Counters, that measures the decay muons from pion and kaon decay coming at wide angles from the decay pipe.

The other major source of background events is NC π^0 production, where one of the gammas from the π^0 decay overlaps the other or is too low energy to be detected. Over 99% of the NC π^0 events are rejected in the appearance analysis, and about 22% are fully reconstructed, which allows the overall number and kinematic distributions to be studied. As seen in Figure 10, the invariant mass distribution is understood very well. The identified π^0 events in the data can then be used to extrapolate into the kinematic region of the background. As an example, Figure 14 shows the asymmetry distribution of the two photons for identified π^0 events for data and Monte Carlo; the good agreement for events with large asymmetry gives confidence that this background can be understood.

Another handle on the background is the energy distribution of the various components as shown in Figure 15 where the background is summed with a signal for a high (low) Δm^2 value of 1 (0.4) eV^2 . The intrinsic ν_e events show a clear high energy tail which can be identified and the misidentified π^0 events are narrower in energy than an oscillation signal, so a fit to the energy distribution can be used to enhance the sensitivity to an oscillation signal. The MiniBooNE sensitivity has been estimated by performing such energy-dependent fits to simulated data with no underlying oscillation signal. Figure 16 shows the expected 90%, 3σ , and 5σ MiniBooNE exclusion regions for an underlying null signal; Figure 17 shows how well an oscillation signal can be measured at either low or high Δm^2 .

At the current time MiniBooNE has collected about 2.5×10^{20} protons on target. The data collection rate is steadily improving as the Booster accelerator losses are reduced. Many improvements are being implemented into the Booster and LINAC which not only help MiniBooNE but

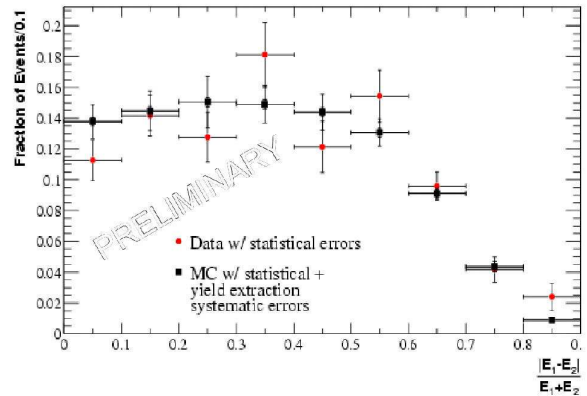


Figure 14. Fraction of NC single π^0 events as a function of the asymmetry of the reconstructed gamma energies. The event fraction in each bin is extracted via a fit to the invariant mass plot for events in that bin. The background and “signal” shapes used in the fit are from a MC-based parameterization.

also the Tevatron and NuMI experiments. The MiniBooNE collaboration plans to “open the ν_e appearance box” when the analysis has been substantiated and when sufficient data has been collected for a definitive result; this is expected to be sometime in 2005.

2.3. Future Plans and Possible Follow-up Experiments

Whether or not MiniBooNE sees an oscillation signal in neutrino running mode, it is also important to run with antineutrinos. Antineutrino results will both directly address the LSND anomaly, which was associated with a $\bar{\nu}_\mu \rightarrow \bar{\nu}_e$ signal; and allow investigations of possible CP or CPT violation effects. If MiniBooNE sees a signal in neutrino mode, then it will be important to see if the mixings and Δm^2 values are the same for incident antineutrinos. The antineutrino event rate is about a factor of four lower than the neutrino rate for a given number of protons on target, but the π^0 and intrinsic ν_e backgrounds are significantly lower. Because of these effects, one needs

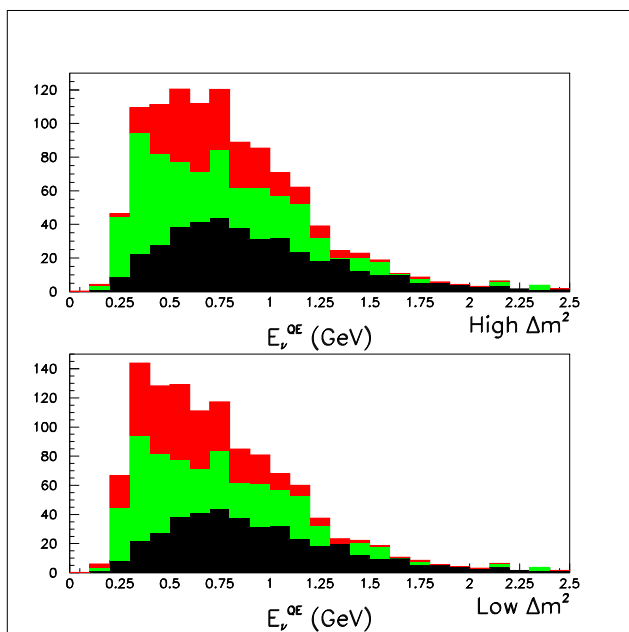


Figure 15. Summed event energy distribution for the oscillation signal and backgrounds. The bottom black area is the intrinsic ν_e background events, the middle light region is the NC π^0 events, and the top area is the oscillation events for 1.0 (top) and 0.4 (bottom) eV^2 . The data sample corresponds to 1×10^{21} protons on target.

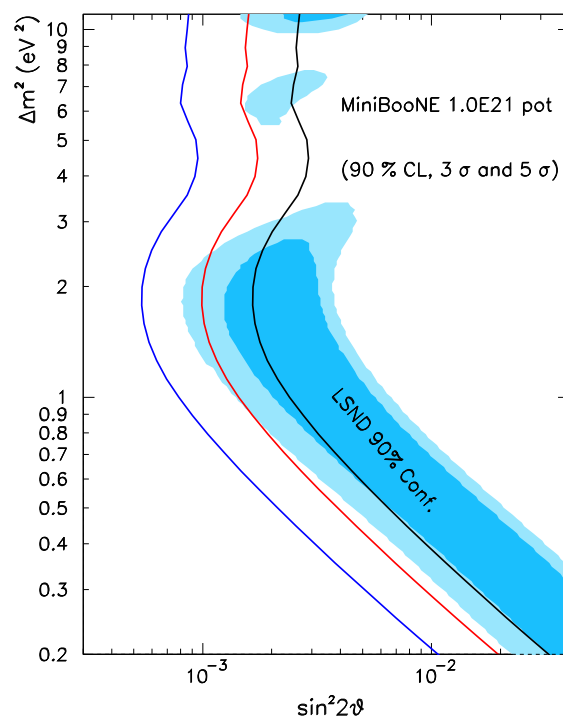


Figure 16. Estimate of the MiniBooNE oscillation sensitivity for 1×10^{21} protons on target using fits to the event energy distribution including signal and backgrounds. The dark (light) areas are the LSND 90% (99%) CL allowed regions. The three curves give the 90%, 3σ , and 5σ sensitivity regions for MiniBooNE.

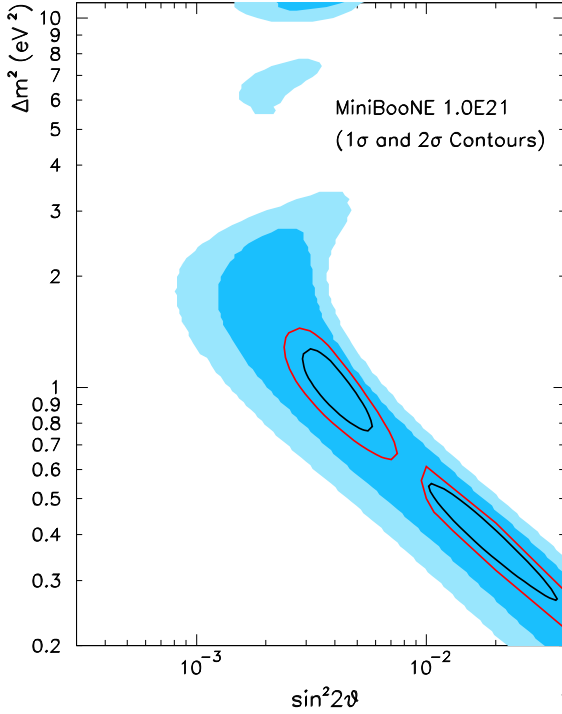


Figure 17. One and two sigma contours for an oscillation signal with $\Delta m^2 = 0.4$ or 1.0 eV^2 for a data sample corresponding to 1×10^{21} protons on target.

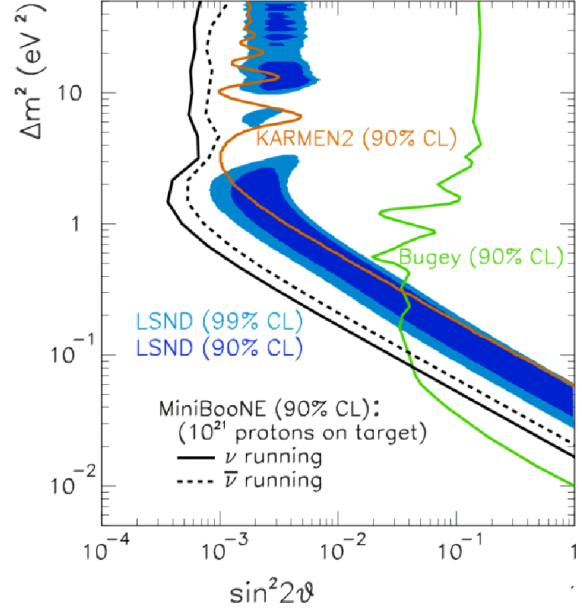


Figure 18. Estimate of the MiniBooNE oscillation sensitivity at 90% CL for 1×10^{21} protons on target for neutrino and antineutrino running. The dark (light) areas are the LSND 90% (99%) CL allowed regions. Also, shown are the 90% CL limits from the KARMEN2 and Bugey experiments.

to run twice as long in antineutrinos to reach similar sensitivity as for neutrino running as shown in Figure 18.

If MiniBooNE sees an oscillation signal, the planned next step is to add a second detector at an optimal location (2 km for low Δm^2 or 0.25 km for high Δm^2) in order to explore the oscillation parameters; this upgrade is referred to as the “BooNE” experiment. This two (or more) detector setup would allow precision measurements of the parameters, Δm^2 to $\pm 0.014 \text{ eV}^2$ and $\sin^2 2\theta$ to ± 0.002 . Figure 19 shows an example measurement for an underlying Δm^2 value of 0.3 eV^2 . With this sensitivity, there are many questions concerning the oscillation signal that the BooNE experiment will explore. The first question to address is if the signal is consistent with the L/E

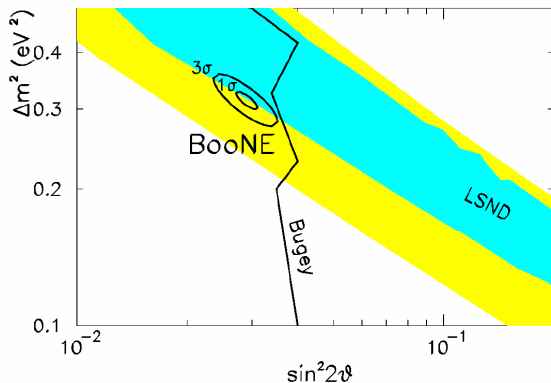


Figure 19. Example of a two detector BooNE measurement for an underlying oscillation scenario with $\Delta m^2 = 0.3 \text{ eV}^2$. The one and three sigma regions are displayed.

behavior expected for neutrino oscillations. In the (3+n) type sterile neutrino models, BooNE can determine how many separate Δm^2 there are. Finally, with two detectors, BooNE can perform a much more precise ν_μ disappearance search that would directly probe for indications of oscillations to sterile neutrinos.

A positive MiniBooNE signal will also prompt investigations by other experiments at Fermilab, BNL, CERN, and JPARC. It will be important to map out the oscillations related to all three types of active neutrinos, ν_e , ν_μ , and ν_τ , in this high Δm^2 region with both appearance and disappearance measurements. A $\nu_\mu \rightarrow \nu_\tau$ appearance experiment using, for example, an Opera-style emulsion detector could explore this region but would require a higher energy neutrino beam to overcome the τ production threshold effects; the NuMI 8 GeV medium energy beam is a possibility.

In conclusion, neutrinos have provided many surprises over the past decade and will most likely continue to do so. Although the “neutrino standard model” can be used as a guide, the future direction for the field will be determined by what we discover from experiments. The possibility that

sterile neutrinos exist may open up a whole new area to explore.

REFERENCES

1. The MiniBooNE Collaboration consists of scientists from the following institutions: University of Alabama; Bucknell University; University of Cincinnati; University of Colorado; Columbia University; Embry-Riddle Aeronautical University; Fermi National Accelerator Laboratory; Indiana University; Los Alamos National Laboratory; Louisiana State University; University of Michigan; and Princeton University. More information may be found at <http://www-boone.fnal.gov/>.
2. P. C. de Holanda and A. Y. Smirnov, arXiv:hep-ph/0307266.
3. G. C. McLaughlin, J. M. Fetter, A. B. Balantekin and G. M. Fuller, Phys. Rev. **C59**, 2873 (1999) [arXiv:astro-ph/9902106]; D. O. Caldwell, G. M. Fuller and Y. Z. Qian, Phys. Rev. **D61**, 123005 (2000) [arXiv:astro-ph/9910175].
4. K. N. Abazajian, Astropart. Phys. **19**, 303 (2003) [arXiv:astro-ph/0205238]; G. Steigman, arXiv:hep-ph/0309347; J. F. Beacom, N. F. Bell and S. Dodelson, arXiv:astro-ph/0404585.
5. S. Hannestad, JCAP **0305**, 004 (2003) [arXiv:astro-ph/0303076].
6. M. Sorel, J. M. Conrad and M. Shaevitz, arXiv:hep-ph/0305255.
7. A. A. Aguilar-Arevalo *et al.* (MiniBooNE Collaboration), “The MiniBooNE Run Plan”, Nov., 2003, <http://www-boone.fnal.gov/publicpages/runplan.ps.gz>.
8. The HARP Experiment at CERN, See <http://harp.web.cern.ch/harp/>.
9. The E910 Experiment at BNL, See <http://www.phy.bnl.gov/~e910/html/home.html>.